CrossMark
click for updates

On the development of a new nonequilibrium chemistry model for Mars entry

R. L. Jaffe[1], D. W. Schwenke[2], G. M. Chaban[3],
NASA Ames Research Center, Moffett Field, CA 94035-1000

D. K. Prabhu[4]
Analytical Mechanics Associates, Inc., Moffett Field CA 94035-1000

C. O. Johnston[5]
NASA Langley Research Center, Hampton, VA 23681

and

M. Panesi[6]
University of Illinois at Urbana-Champaign, Urbana, IL 61801

This paper represents a summary of results to date of an on-going effort at NASA Ames Research Center to develop a physics-based non-equilibrium model for hypersonic entry into the Martian atmosphere. Our approach for the determination of reaction rate coefficients is to first compute potential energy surfaces based on accurate solutions of the electronic Schrödinger equation and then use quasiclassical trajectory calculations to obtain reaction cross sections and rate coefficients based on these potentials. We have presented new rate coefficients for N_2 dissociation and CO dissociation and exchange reactions. These results illustrate shortcomings with some of the rate coefficients in Park's original T-T_v model for Mars entries and with some of the 30-45 year old shock tube data. We observe that the shock tube experiments of CO + O dissociation did not adequately account for the exchange reaction that leads to formation of C + O_2. This reaction is actually the primary channel for CO removal in the shock layer at temperatures below 10,000 K, because the reaction enthalpy for exchange is considerably lower than the comparable value for dissociation. The rate coefficients reported herein should reduce the uncertainty in modeling hypersonic flows expected for entry of heavy spacecraft into the Martian atmosphere.

I. Introduction

NASA has plans to land increasingly heavier payloads on Mars over the next two decades, as preparation for a manned Mars mission. To date, the heaviest object that has been safely landed on Mars is about one metric ton. The safe landing of payloads on Mars is difficult owing to the low atmospheric density. The Martian atmosphere is 96% CO_2 with 1.9% each N_2 and Ar by volume and other minor constituents [1] and the average atmospheric pressure at the surface is only 0.008 bar [2]. Depending on the entry architecture of the proposed NASA missions, the entry speeds will be 5-8 km/s and the equilibrium temperature of the bow shock layer will be 4,000-8,000 K. The shock layer around the entry vehicles is predicted to be chemical and thermal nonequilibrium, with the translation temperature, T, peaking at 12,000-

---

[1] Research Scientist, Aerothermodynamics Branch, NASA Ames Research Center, Mail Stop 230-3, Moffett Field, CA 94035-1000, Associate Fellow AIAA

[2] Research Physicist, Computational Physics Branch, NASA Ames Research Center

[3] Research Physicist, Computational Physics Branch, NASA Ames Research Center

[4] Senior Scientist, Entry Systems and Technology Division, NASA Ames Research Center, Mail Stop 229-x, Moffett Field, CA 94035-1000, Associate Fellow AIAA

[5] Aerospace Engineer, Aerothermodynamics Branch, NASA Langley Research Center, Research Directorate, Member AIAA

[6] Assistant Professor, Aerospace Engineering Dept., University of Illinois at Urbana-Champaign, Member AIAA

1

20,000 K and internal temperature, T_{int}, of the gases rising slowly in time until it is equal to T and local thermal equilibrium is achieved. Under most of these entry conditions CO_2 will be completely dissociated in the shock layer; thus the important species for Mars nonequilibrium chemistry will be CO and atomic oxygen. For some mission scenarios with the entry speed less than 5 km/s, CO_2 will not be completely dissociated in the shock layer. For the range of entry speeds considered the degree of ionization is predicted to be less than 0.5%. The composition of the Venusian atmosphere (96.5% CO_2 and 3.5% N_2 [3]) is similar to Mars, but the pressure is much greater. At altitudes of 50-65 km, the pressure and temperature of Venus and Earth atmospheres are similar [4]. Owing to greater gravitational forces, the entry speed of planned Venusian entries will be greater than 10 km/s [5,6].
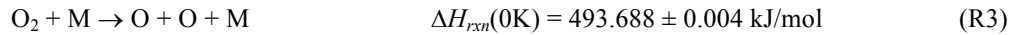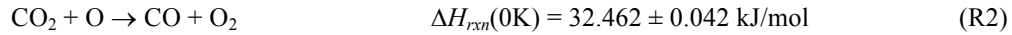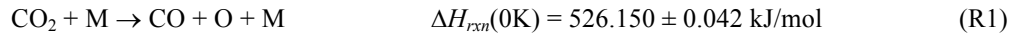
In order to predict the expected heat flux that the entry vehicle will experience, Computational Fluid Dynamics (CFD) and radiative transport simulations using a reacting gas model are performed. The predicted convective and radiative heat loads along the entry trajectory are then used to design the thermal protection system. The two-temperature (T-T_v) nonequilibrium chemistry paradigm introduced by Park [7-10] in the 1980s is still widely used today for CFD simulations of flow fields surrounding spacecraft entering planetary atmospheres. The vibrational temperature (T_v) also describes the electronic state and free electron temperatures and the rotational temperature is assumed equal to T. The relationship between T and T_v is given by a first-order relaxation expression based on the Landau-Teller model [11,12]. Park made the additional *ansatz* that the temperature dependence of molecular dissociation reaction rate coefficients depends on an average temperature (T_{av}) which is defined as the geometric mean of T and T_v ($T_{av} = [T \times T_v]]^{1/2}$). When T = T_v, the regular Arrhenius rate coefficient expression for dissociation reactions holds and the parameters of that expression are used to describe the reaction kinetics when T ≠ T_v. In the Landau-Teller model, an additional relaxation equation is used to control the rate of relaxation of T_v toward thermal equilibrium. The so-called vibrational relaxation time τ_v is the parameter required for the Landau-Teller model, and values of that parameter are required for every molecule-collision partner pair. Additional parameters needed for the T-T_v model are the thermochemical enthalpy and entropy for each of the atomic and molecular species, and transport parameters for mass and energy diffusion.

Most of the experimental data used to formulate the T-T_v models was obtained from experiments and flight tests carried out more than 30 years ago. Over the years, the sets of species and elementary chemical reactions described in these models have been modified and the parameters (*e.g.*, rate coefficients, transport coefficients and relaxation constants, etc.) have been refined based on new experimental data and measurements from flight tests and high-enthalpy ground-based facilities. However, most of the experimental data still being used in the T-T_v models was obtained from experiments and flight tests carried out more than 30 years ago. Park's chemistry models for Earth entry [13] and for Mars and Venus entry [14] (referred herein as Park94) are still the *de facto* standard in the aerothermodynamics community. In 2014, Johnston and Brandis [15] published an update to Park94 (referred to as Johnston2014) which contains updated reaction rate coefficients empirically adjusted to improve the agreement between CFD-radiative transport calculations and measurements carried out in the Electric Arc Shock Tube (EAST) facility at NASA Ames Research Center.
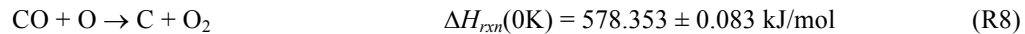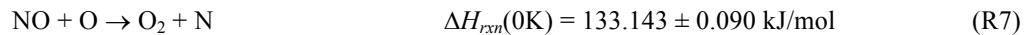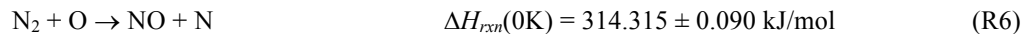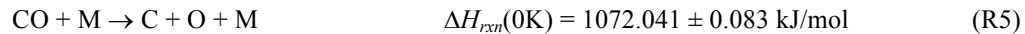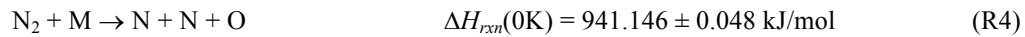
Concurrently, a multi-year project has been underway at Ames to develop a new so-called "physics-based" nonequilibrium chemistry model for Mars entry based on computational physics and chemistry and validated through measurements in EAST [16] by using the computational tools DPLR [17] and LAURA [18] for flowfield simulations and NEQAIR [19] and HARA [20] for radiation modeling. The goals of this project are to improve our understanding of the physical processes in the shock layer around entry vehicles and in ground test facilities, improve the accuracy of the physical and chemical models and ultimately to reduce the modeling uncertainty in predictions of the convective and radiative heating spacecraft will experience during Mars entry. This paper is a status report of results from that project.

The most important components of nonequilibrium chemistry models for hypersonics are rate coefficients for the dissociation and exchange reactions involving the atmospheric species at high temperatures. If the spacecraft has an ablating heat shield, one must also consider interaction between ablation products (often these are carbonaceous species such as C, C_2, CO, C_3, C_2H, etc.) and the atmospheric species. The following reactions constitute the set required to model Mars entries without accounting for ablation. As mentioned above, the Mars atmosphere is mostly CO_2 with a small amount of molecular nitrogen. Reaction R1 describes the initial reaction that occurs in the shocked gas: namely, dissociation of CO_2 with M being the collision partner (CO_2, N_2, or Ar). After sufficient mole fractions of CO and atomic oxygen are attained, the exchange reaction R2 dominates, because the activation energy for this reaction is much less than the energy required for dissociation. R2 has an estimated energy barrier of
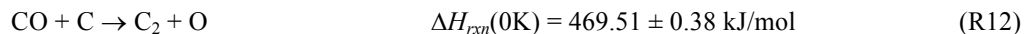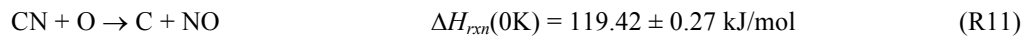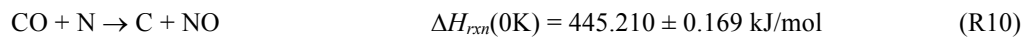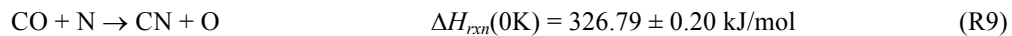
between 205 and 285 kJ/mol [21,23] and the O_2 formed by this reaction is also more easily dissociated than is CO_2. In fact, for entry speeds greater than 5 km/s, nearly all the CO_2 is dissociated immediately after the shock. And the dominant shock layer species become CO and O.

$$CO_2 + M \rightarrow CO + O + M \qquad \Delta H_{rxn}(0K) = 526.150 \pm 0.042 \text{ kJ/mol} \qquad \text{(R1)}$$

$$CO_2 + O \rightarrow CO + O_2 \qquad \Delta H_{rxn}(0K) = 32.462 \pm 0.042 \text{ kJ/mol} \qquad \text{(R2)}$$

$$O_2 + M \rightarrow O + O + M \qquad \Delta H_{rxn}(0K) = 493.688 \pm 0.004 \text{ kJ/mol} \qquad \text{(R3)}$$

At that point, reactions that remove CO and N_2 take over. The dissociation reactions (R4 and R5, respectively) are slow because the N_2 and CO bond energies are quite large. However, due to the abundance of atomic oxygen, exchange reactions offer an effective lower-energy mechanism for removing N_2 and CO. For N_2, the two elementary reactions of the Zel'dovich mechanism (R6 and R7) convert N_2 to NO and O_2. For CO reaction with atomic oxygen (R8) produces $C + O_2$.

$$N_2 + M \rightarrow N + N + O \qquad \Delta H_{rxn}(0K) = 941.146 \pm 0.048 \text{ kJ/mol} \qquad \text{(R4)}$$

$$CO + M \rightarrow C + O + M \qquad \Delta H_{rxn}(0K) = 1072.041 \pm 0.083 \text{ kJ/mol} \qquad \text{(R5)}$$

$$N_2 + O \rightarrow NO + N \qquad \Delta H_{rxn}(0K) = 314.315 \pm 0.090 \text{ kJ/mol} \qquad \text{(R6)}$$

$$NO + O \rightarrow O_2 + N \qquad \Delta H_{rxn}(0K) = 133.143 \pm 0.090 \text{ kJ/mol} \qquad \text{(R7)}$$

$$CO + O \rightarrow C + O_2 \qquad \Delta H_{rxn}(0K) = 578.353 \pm 0.083 \text{ kJ/mol} \qquad \text{(R8)}$$

Other exchange reactions (R9-R12) involving atomic nitrogen and carbon convert CO to CN, NO and C_2. These are also important because CN and C_2 are responsible for intense photoemissions observed in the visible and UV. The CN, NO and C_2 molecules formed by reactions R9-R12 can also undergo collisional dissociation.

$$CO + N \rightarrow CN + O \qquad \Delta H_{rxn}(0K) = 326.79 \pm 0.20 \text{ kJ/mol} \qquad \text{(R9)}$$

$$CO + N \rightarrow C + NO \qquad \Delta H_{rxn}(0K) = 445.210 \pm 0.169 \text{ kJ/mol} \qquad \text{(R10)}$$

$$CN + O \rightarrow C + NO \qquad \Delta H_{rxn}(0K) = 119.42 \pm 0.27 \text{ kJ/mol} \qquad \text{(R11)}$$

$$CO + C \rightarrow C_2 + O \qquad \Delta H_{rxn}(0K) = 469.51 \pm 0.38 \text{ kJ/mol} \qquad \text{(R12)}$$

All of these reactions are written in the endothermic direction. In the flowfield, however, they can occur in either that direction or in the reverse (exothermic) direction. The ratio of the forward and reverse reaction rate coefficients is equal to the equilibrium constant (which is determined from the change in Gibbs free energy for the reaction), so the rate coefficient of a reaction only has to be specified in one direction.

The values for the reaction enthalpies given above are determined using the Active Thermochemical Tables (ATcT) developed by Ruscic and coworkers at Argonne National Laboratory [24-27]. ATcT uses a network approach to assigning formation enthalpies at 0 K and 298 K for individual atomic and molecular species. In contrast, older compendia of thermochemical data such as CEA [28], JANAF [29] and Gurvich [30] use a sequential strategy of adding one new species at a time to an existing set. The network approach simultaneously optimizes the complete set based on some initial set of energies. It is readily expandable as new data for existing species and data for new species become available. In contrast, it is not as easy to add new species or update tables for existing species as in the other compendia. Currently, the ATcT database contains many species of interest to hypersonics that are not present in other thermochemical databases, such as highly reactive molecules like C_2H_3, C_2H_5, N_2H and N_2H_3 that are important species for modeling propellants and ablating surfaces. For Mars entry, the main differences between ATcT and JANAF formation enthalpies are the increased precision and smaller standard errors. In

addition, ATcT incorporates the newer value for the C_2 heat of formation, resulting in a -9.0 kJ/mol change from the JANAF value $\Delta_f H^o(0K)$ = 820.26 kJ/mol ATcT and 829.3 kJ/mol JANAF). Large differences between ATcT and JANAF also exist for C_2H, C_2H_2 and C_3, which are used in modeling ablation. To compute the equilibrium constants over the full range of temperatures required for simulating entry flows, the enthalpy and entropy have to be determined over this temperature range. This is accomplished for molecules by computing the specific heat, $C_P(T)$ using the rovibrational energy levels for all the bound electronic states. These energy levels can be determined using the quantum chemistry calculations described in the next section.

In all, the new nonequilibrium chemistry model for use in CFD simulations of Mars entry flows will require: (1) parameters for Arrhenius expressions for thermal rate coefficients for reactions R1-R12, (2) values for thermodynamic functions such as enthalpy and entropy that are used to compute equilibrium constants for these reactions, (3) internal energy relaxation parameters to model the evolution of internal temperatures and (4) transport coefficients for mass and energy diffusion throughout the flowfield for all pairs of colliding species. In addition, spectroscopic constants for optical and molecular absorption and emission transitions that occur in the shock-heated gases are needed to compute the radiative heat flux impinging on the spacecraft. In this paper we concentrate on (1), the determination of rate coefficients for reactions relevant to Mars entry.

The paper is organized as follows: section II is a short description of the computational physics and chemistry methods used to determine parameters for the nonequilibrium chemistry model, III contains new values for rate coefficients, IV describes tests of the chemistry data in Computational Fluid Dynamics (CFD) calculations for typical Mars entry conditions, and V presents our recommendations and conclusions.

II. Computational Chemistry Methods

Physics-based modeling of hypersonic flows is predicated on the availability of chemical reaction rate coefficients and cross sections for the collisional processes. This approach has been built around the use of quantum mechanical methods to model the interaction between the colliding particles and is described in detail in the work of Jaffe *et al*. [27] In this approach, an *ab initio* potential energy surface (PES) is computed by solving the electronic Schrödinger equation for many geometric arrangements of the atoms that comprise the colliding particles. Given a PES, collision cross sections are determined for that PES using classical, semiclassical or quantum mechanical scattering methods. As the calculation of the energy for each geometry is computationally intensive, the set of geometry and energy data must be fit to some analytic function which is used as input for the scattering calculations. In order to obtain cross sections of sufficient accuracy, the *ab initio* quantum chemistry calculations should provide relative energies (*i.e.,* between geometries) of an accuracy $\pm$ 5 kJ/mol or less. This presents a formidable challenge, as discussed in ref. 31.

For computing rate coefficients of chemical reactions we primarily use classical scattering method called quasiclassical trajectory calculations (QCT). This method simulates individual collisions using Hamilton's equations of motion, with initial conditions selected by Monte Carlo sampling of appropriate distributions for geometric orientation, vibrational and rotational phase, impact parameter and collision energy. Each individual collision is a trajectory and the initial vibration and rotation energies of reactant molecules are chosen to represent quantized rovibrational levels. The trajectory starts with separated reactants moving toward each other and continues until the products of the collision are well separated. The trajectory can represent an inelastic collision (the reactant species are in different rovibrational levels), a dissociation reaction (one of the initial molecules is now two separated atoms) or an exchange reaction (new molecules have been formed). A large batch of trajectories are computed for each set of initial conditions and the cross section for a specific outcome (for example, dissociation) is proportional to $N(i)/N_{total}$, where N_{total} is the number of trajectories computed and $N(i)$ is the number which have that desired outcome. In these calculations, N_{total} is on the order of 10^5 to 10^7 and the statistical sampling error is on the order of $N(i)^{-1/2}$. Thermal reaction rate coefficients are computed by integrating the cross sections over a range of collision energies with Maxwell-Boltzmann weighting. Cross sections can be computed for specific molecular rovibrational energy levels or these energy levels can be sampled from a thermal Boltzmann distribution. A lengthy description of the QCT method is also given in ref. 31.

If the flow is in thermal non-equilibrium, the translational, vibrational and rotational energy modes can be represented in different ways: (1) the rovibrational energy modes can be described by an internal temperature (T_{int}) that is distinct from the translational temperature T; (2) three different temperatures (for

translation, vibration and rotation) can be used to describe the distributions (for example, the Park94 T-T_v model with $T_r = T$); or (3) the populations of individual rovibrational energy levels can be determined by solving the Master Equation [32]. The full Master Equation is the most accurate method for describing the details of each reaction, but it is exceedingly difficult to carry out. The diatomic molecular species involved in Earth and Mars entry flows all have between 7000 and 13,000 rovibrational levels, so the number of state-to-state rate coefficients (and thus the dimensionality of the Master Equation) is quite large. Recent research in the development of coarse-grained models [33-35] has led to strategies for combining the rovibrational levels into large groups, so that the detailed reaction kinetics and energy relaxation of each molecule can be accurately described by 5-10 independent groups of energy levels, each with their own rate coefficients. The coarse-grained Master Equation approach is an attractive avenue of research, but it is beyond the scope of the present study.

The *ab initio* potentials can also be used for simulating absorption and emission spectra. For molecules, the energy levels of bound rovibrational levels must be computed for both upper and lower states for electronic transitions, along with the expectation value of the appropriate operator (electric dipole moment for IR spectra, electric dipole transition moment for electric dipole allowed electronic spectra, etc.) over the entire grid of geometries. For diatomic molecules, the semiclassical WKB approximation [36] is often used to compute the full set of rovibrational levels. Alternatively, solution of the Schrodinger equation for the motion of atoms under the influence of the electronic potential [37,38] can be used for all types of molecular spectra.

III. Results for reaction rate coefficients

Using the results of the calculations described above, thermal reaction rate coefficients and molecular thermodynamic properties have been computed. Where possible, in order to provide some assurance that the calculations are sufficiently accurate, these rate coefficients are validated by comparison with various experimental measurements. The results of some of these calculations are presented below for species and chemical reactions that are expected to play a significant role under typical Mars entry conditions.

To identify the most important reactions for study, we used an Uncertainty Quantification (UQ) method [39] to determine which reactions control the magnitude of the radiative heat flux and the time for the flowfield to reach thermal equilibrium after the shock [40]. We carried out a large number of flow calculations for a 1-dimensional shock with random selection of the Arrhenius parameters and vibrational relaxation times. For each of these parameters, we randomly selected the value within the interval $p/10 \leq p_i \leq 10*p$, where p is the value of that parameter in the Park94 nonequilibrium model and p_i is the value selected for the *ith* trial. From these trials we computed the integrated intensity of the CO 4th positive radiation and the distance after the shock when the flow temperature had relaxed to $T/T_{eq} = 1.05$. The principal source of radiative heating for Mars entry at speeds of 5-8 km/s is from the CO 4th positive band system in the vacuum ultraviolet (VUV) [11], it is not surprising that the production of CO by dissociation of CO_2 (R1 and R2) and the dissociation and exchange reactions that remove CO (R5 and R8) are found to be most important in controlling the radiative heating. In addition, the UQ study found R9-R11 are also important reactions for controlling the equilibration of the flow. These are the exchange reactions that regulate the mole fractions of CN and NO. The results are summarized in Table 1 for the free stream condition 96% CO_2 and 4% N_2 at 3 Pa and 300K with a shock speed of 7.75 km/s, which approximates the Mars Pathfinder mission entry. In light of these findings, we prioritized our work as follows: evaluate rate coefficients for (1) CO dissociation by collision with O and CO (R5), (2) the exchange reaction between O and CO (R8), and (3) the exchange reactions involving CO, CN and NO (R9-11). The dissociation reactions are most important because the relative efficiencies of different collision partners (*e.g.*, Ar, CO and O) in promoting dissociation are not well known. Park94 [14] uses factors of 1, 5 and 15, respectively for Ar, CO and O, while an earlier compendium of gas phase reaction rates by Baulch *et al.* [41] recommends factors of 1, 1-2 and 15 for CO dissociation (R5).

5

Table 1. Major results of the Uncertainty Quantification study for Mars Entry:
Important reactions that determine the radiative flux due CO 4th Positive emission
and the time to reach chemical and thermal equilibrium after the shock

Reaction	Sensitivity to Radiative Flux	Sensitivity to Equilibration Time
$CO + O \rightarrow C + O + O$ (R5)	55%	48%
$CO + CO \rightarrow C + O + CO$ (R5)	25%	10%
$CN + O \rightarrow C + NO$ (R11)	9%	24%
$CO + O \rightarrow C + O_2$ (R8)	4%	8%

A different approach was followed by Johnston and Brandis (Johnston2014 [15]) to derive their modification of the Park94 [14] chemistry model. Their objective was to enable DPLR-NEQAIR and LAURA-HARA simulations to better match the spectral intensities measured in EAST for CO 4th positive and CN violet emission for the following conditions: 6-8 km/s shock speed and 0.1 to 1.0 torr pressure in a 96% CO_2 and 4% N_2 gas mixture. No CO_2 IR emission was observed for those conditions, so CO_2 dissociation (R1) was assumed to be complete. Johnston and Brandis found that the computed CO radiative intensity was too high relative to the EAST measurements and recommended increasing the rate coefficient for CO dissociation (R5) by a factor of 5.2 to reduce the mole fraction of CO in the shock layer. In their analysis, they kept the relative efficiencies of Ar, CO and O used in the Park94 model [14]. They also found adjustments in the rate coefficients for the CO + N (R9) and CN + O (R11) exchange reactions by factors of 10 and 0.1, respectively, were needed to match the observed intensity for the CN violet bands. Finally, adjustments were made to the rate coefficients for Zel'dovich exchange (R6 and R7) and for C_2, CN and NO dissociation. Thus, they adjusted most of the reaction rate coefficients that the UQ study found to be important for controlling the CO radiative emission and equilibration time.

In the last few years, *ab initio* potential energy surfaces and QCT thermal rate coefficients have become available for O_2 and N_2 dissociation (R3 [42-51] and R4 [52-55], respectively), and the Zel'dovich exchange reactions (R6 [56-61] and R7 [62-64]). In addition, Schwenke, Jaffe and Chaban (denoted Schwenke2016) [65] have computed PESs and thermal rate coefficients for CO + M dissociation (R5) with M = Ar and O and the CO + O exchange reaction (R8). These researchers are also applying this approach to CO dissociation with M = CO. The CO + N exchange reactions (R9-R11) have also been the subject of recent computational studies [66-69]. Thus, in the near future a consistent set of rate coefficients will be available most of the chemical reactions that take place in the shock layer during Mars entries. Rate coefficients for R4, R5 and R8 have been computed from the appropriate PESs and those results are presented and discussed in this section. We plan to use some of these PESs for other reactions to obtain similar rate coefficient calculations for R3, R6, R7 and R9-11.

Results for N_2 dissociation with M = N_2 and N, the CO dissociation with M = Ar and O and CO + O exchange reactions are presented to illustrate our approach and to illustrate the problems of validating the results against experimental measurements. For N_2 dissociation, rate coefficients have been measured in shock tube experiments by Appleton [70] for 8000 K < T < 15,000 K, Hanson [71] for 5700 K < T < 12,000 K, Hornung [72] for 6000 K < T < 14,000 K and Roth [73] for 3390 < T 6435 K. Common practice in these shock tube experiments was to use a nitrogen-noble gas mixture (usually argon) and to monitor the decreasing N_2 mole fraction or increasing N atom mole fraction. The primary chemical kinetics measurements were made for reaction R4 with M = Ar with a small initial N_2 mole fraction. The measured N_2 + Ar rate coefficient data were fit to Arrhenius expressions $k_{rxn}(T) = A \times exp(-T_{rxn}/T)$ or $k_{rxn}(T) = B \times T^{-n} \times exp(-D_0/RT)$. In these expressions, A, T_{rxn}, B and n are adjustable parameters and D_0/R is the diatomic dissociation energy in Kelvin, measured from the lowest rovibrational level. By varying the initial N_2 mole fraction, rate coefficients for M = N_2 and M = N could be obtained. For these cases, the values of n and T_{rxn} were fixed at the M = Ar values and only parameters A and B were adjusted when fitting the data to an Arrhenius expression. Some of the experiments (*e.g.*, ref. 71 and 72) used pure N_2 gas, and all the Arrhenius parameters for M = N_2 and M = N could be determined by fitting the shock tube data. In general, the fits to the experimental data were considered to have an uncertainty of ±20-30% for M = Ar and ~±50% for M = N_2 and M = N.

Potential energy surfaces for N_2 + N_2 (N4) and N_2 + N (N3), with all species in their ground electronic states ($^1\Sigma_g^+$ for N_2 and ^4S for N), have been generated at NASA Ames by Schwenke, Jaffe and

Chaban [52,53] using *ab initio* quantum mechanical calculations (as described in the previous section and in ref. 31). Independently, similar PESs for N4 have been created at the University of Minnesota by Truhlar, Candler and co-workers [53-55] (in their case, the N3 PES is included as a subset of N4). These N4 and N3 PESs are based on similar quantum chemistry methods, in that they *approximate* the same Multi-Reference Configuration Interaction (MRCI) solution. However, they used quite different geometry grids and strategies for creating the analytic representation to faithfully represent the *ab initio* energies. Thermal dissociation rate coefficients for $N_2 + N_2$ and $N_2 + N$ collisions for temperatures between 7500 K and 30,000 K have been computed by both research groups using the QCT method. These dissociation rate coefficients are compared in Figures 1 and 2, for $N_2 + N_2$ and $N_2 + N$, respectively. Also shown are the fits to the experimental rate coefficients described above. For $N_2 + N_2$ (Figure 1), the QCT results based on the NASA and UMN potentials are in close agreement over the entire temperature range (8000-30,000 K). They also match the Park94 model and Roth measurements in magnitude and slope for temperatures up to ~10,000 K. For higher temperatures, the slope of the Park rate coefficient becomes lower, indicating curvature in the Arrhenius plot. The Appleton result agrees fairly well with the QCT rate coefficients and exhibits similar slope over the full temperature range of that experiment. However, the Hornung and Hanson experimental data have lower slopes and are only in good agreement with the QCT calculations at ~10,000 K. For $N_2 + N$ (Figure 2), The QCT results using the NASA PES agree quite well in magnitude and slope with the Appleton data. Hornung data agree fairly well with the QCT and Appleton data at higher temperatures, but exhibit a different slope. The Hanson rate coefficients are too high by a factor of 4. The rate coefficient in the Park94 model is also too high, by a factor of 2.5. Figure 3 shows the rate coefficient ratios for $k(N_2+N)/k(N_2+N_2)$ as a function of temperature. The QCT values, using the NASA PES, decrease from 2 at 10,000 K to nearly 1 at 20,000 K, while the Park and Appleton values are constant (by assumption) at a value of 4.3. The Hornung and Hanson values increase with increasing temperature. In the shock layer, $N_2 + N$ collisions dominate the dissociation process, because of their larger rate coefficients.
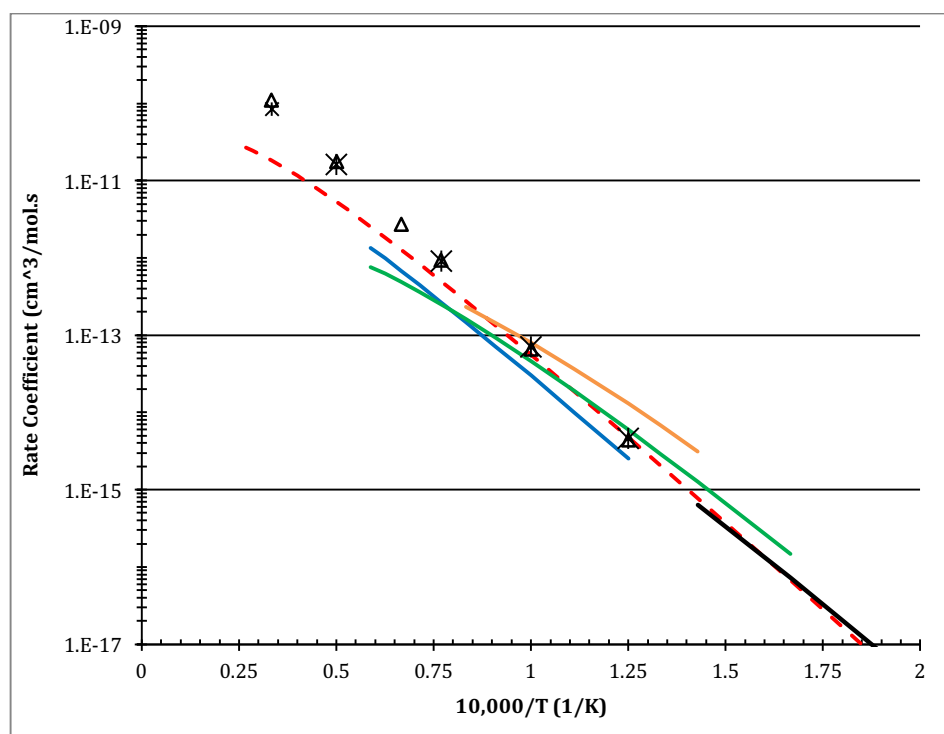

Figure 1. $N_2 + N_2$ **thermal dissociation rate coefficients**. QCT calculations using the NASA Ames [52,53] (black triangles) and University of Minnesota [53] potential energy surfaces (black stars); Park94 [14] (red dashed line); Appleton experiment [70] (blue line); Hanson experiment [71] (orange line); Hornung experiment [72] (green line); Roth experiment [73] (black line). The Arrhenius fits to the experimental data are shown for the temperature range of the experiment.
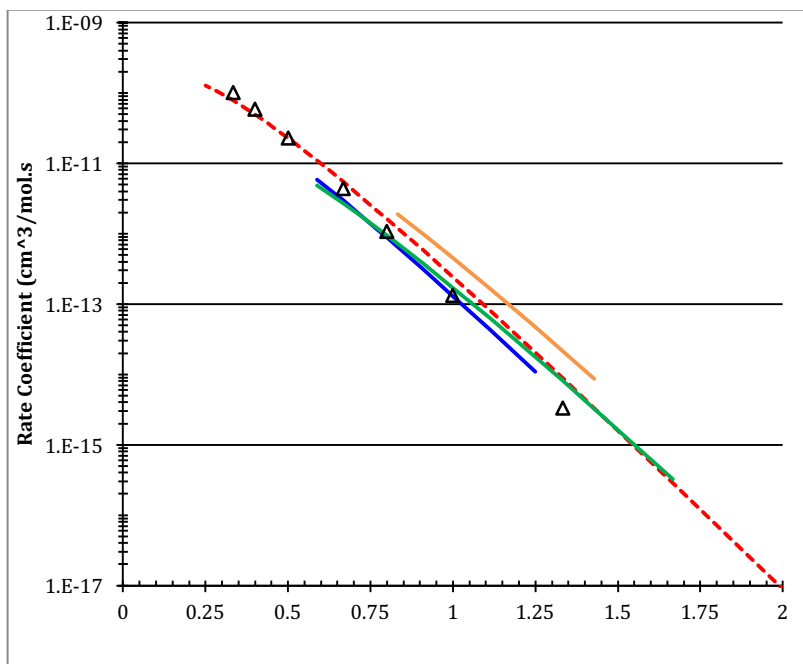
7

Figure 2. **N₂ + N thermal dissociation rate coefficients.** QCT calculations using the NASA Ames [52,53] (black triangles) potential energy surface; Park94 [10] (red dashed line); Appleton experiment [70] (blue line); Hanson experiment [71] (orange line); Hornung experiment [72] (green line). The Arrhenius fits to the experimental data are shown for the temperature range of the experiment.
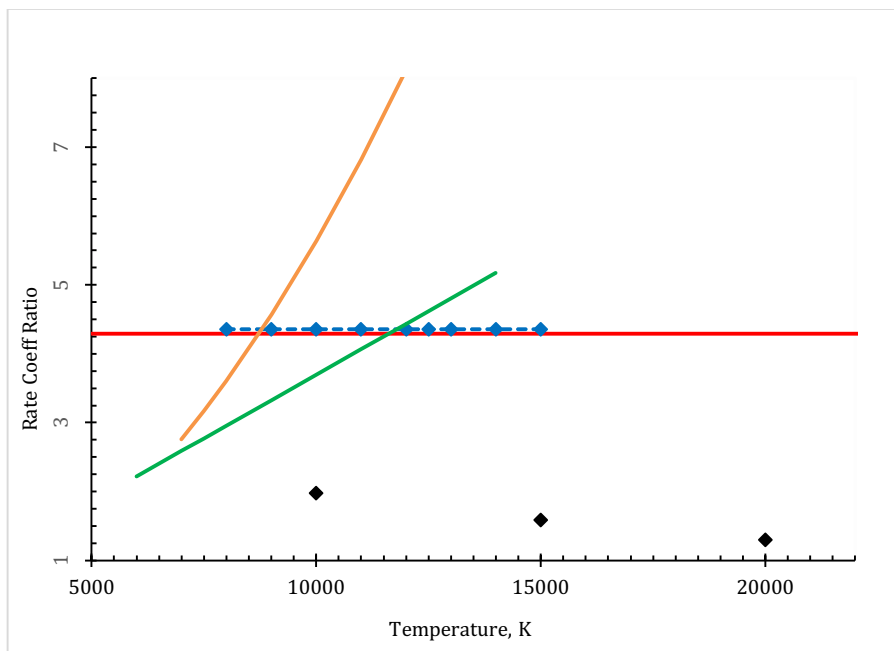

Figure 3. **Ratio of N₂ + N to N₂ + N₂ thermal dissociation rate coefficients.** QCT calculations using the NASA Ames potential energy surface [52,53] (black diamonds); Park94 [14] (red line); Appleton experiment [70] (blue dashed line and diamonds); Hanson experiment [71] (orange line); Hornung experiment [72] (green line).

8

The differences between the QCT rate coefficients and the shock tube results can be attributed to several factors. For example, at T > 10,000 K the gases in the shock tube may not be in thermal equilibrium (as assumed in our calculations) and higher N_2 rovibrational energy levels may be depleted from their thermal populations. Instead, the gas may be in a Quasi Steady State condition (QSS), which results in the reaction rates being lower than the thermal ones. It is also difficult to determine accurate Arrhenius rate coefficient parameters from experiment, because of the limited temperature range and scatter in those data. Appleton [70] used a N_2-Ar gas mixture to measure rates for three dissociation reactions (M = Ar, N_2 and N). Only the M = Ar result had sufficient accuracy to enable determination of the temperature dependence of the dissociation rate coefficient, so he assumed the same temperature dependence for all three reactions. In the QCT calculations, we cover a wider temperature range and can isolate individual reactions to more accurately determine their rate coefficients. However, inaccuracies that may be present in the PES will lead to errors in the rate coefficients. The fact that dissociation rate coefficients from two independent studies [53] of N_2 + N_2 collisions agree so well gives us confidence that the PESs are accurate.

We computed *ab initio* PESs for CO + Ar and CO + O collisions and computed dissociation rate coefficients using these potentials. [65] The CO + Ar PES helps in the calibration of the theoretical methods, as the experimental rate coefficient data for CO + Ar dissociation reaction have been determined with greater accuracy. [74-76] For CO + O, three PESs are needed to describe collisions between the reactants in their ground electronic states (CO $^1\Sigma^+$ and O ^3P). In C_s symmetry, these are designated 1 $^3A'$, 1 $^3A''$ and 2 $^3A''$. All three PESs were computed and QCT rate coefficients were calculated for each of them. The overall thermal rate coefficient is the average of the three individual values. Each of these CO + O PESs describes the dissociation and exchange reactions (R5 and R8). Figure 4 shows the computed CO dissociation rate coefficients for CO + Ar collisions. In that figure, the actual experimental data are shown along with the recommended value from Park94 and the new QCT results. The experimental data are from Davies [74] (actually given for three different measurement techniques), Appleton [75] and Mick and Roth. [76] The QCT values agree quite well with the lower temperature values of Appleton, the higher temperature values of Davies and the values of Mick and Roth. The Park94 values are generally lower by a factor of 3. The CO + O dissociation rate coefficients are shown in Figure 5. Experimental Arrhenius curves are plotted for the Appleton [75] and Hanson [77] experiments, the Park94 model [14], the Johnston2014 modified model [15] and the new QCT data of Schwenke *et al.* [61]. The Appleton and Hanson data are in good agreement where their temperature ranges overlap. In contrast, the Park94 and Johnston2014 rate coefficients have steeper slopes than the experimentally determined fits. Actually Park arbitrarily chose the temperature exponent (-1.0) and scaled the pre-exponential factor to match the Mick and Roth value for CO + Ar at 8000 K and used the same temperature dependence for CO + O. The QCT rate coefficients for CO + O dissociation happen to agree with the Park94 recommendation, but that value is not based on any experimental data. Furthermore, the QCT dissociation rate coefficients are quite different from the experimentally determined values. So there is good agreement between QCT calculation and experiment for the dissociation rate coefficients for CO + Ar, but not for CO + O.

The CO + O exchange reaction (R8) is an alternate chemical pathway in the shock layer for removing CO. The exchange and dissociation reactions are described by the same PESs. So the rate coefficient for this reaction has been determined by QCT calculation [65] and the sum of the dissociation and exchange rate coefficients is shown as open circles in Figure 5. It can be seen that these values agree extremely well with the two sets of experimental rate coefficients over a wide temperature range. When the shock tube experiments were carried out, the exchange reaction was not considered in the data analysis, so it appears that much of the CO removal attributed to dissociation in references 75 and 77 was actually due to the exchange reaction. The rate coefficient given for the exchange reaction in the Park94 model is more than an order of magnitude smaller than the QCT values [64]. The lower endothermicity of the exchange reaction compared to dissociation means that it is most important at lower temperatures where the dissociation rate is extremely low. The combined CO removal rate coefficient (R5+R8), therefore, has a smaller slope than dissociation (R5) alone and agrees well with the experimental data. The rate coefficient parameters for CO + Ar and CO + O (R5 and R8) are given in Table 2. It should be noted that the CO + O dissociation rate coefficient in the Johnston2014 modification of the Park two-temperature model is nearly equal to the QCT dissociation plus exchange rate coefficient at 8000K. However, it is considerably less than the QCT rate coefficient at lower temperatures (i.e., it has a significantly steeper slope than the QCT rate coefficients).
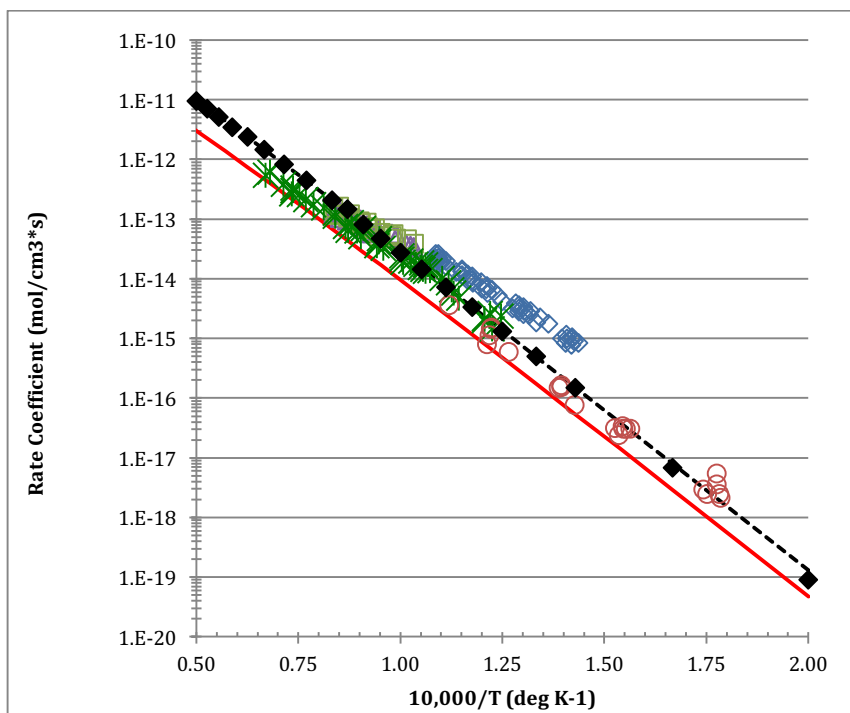
Figure 4. **CO + Ar thermal dissociation rate coefficients.** Data points from various shock tube experiments are plotted along with the Park94 [14] recommendation (red line) and QCT data of Schwenke [65] (black diamonds), computed using the NASA Ames Research Center potential energy surface. The 2-parameter Arrhenius fit of the QCT data (black dashed line) is also shown. Experimental data points are Davies [74] (open blue diamonds, purple triangles and green squares), Appleton [75] (green stars) and Mick and Roth [76] (open brown circles).

Table 2: Parameters for Analytic Representations of CO Dissociation and Exchange Rate Coefficients

| Source	A ($cm^3 molec^{-1} s^{-1}$)	n	T_{rxn} (K)
	CO + Ar		
Schwenke2016[65]	2.781×10^{-5}	-0.85	128741.4
Park94[14]	3.819×10^{-5}	-1	129000
Johnston2014[15]	1.99×10^{-4}	-1	129000
	CO + O dissociation		
Schwenke2016[61]	3.10×10^{-8}	0.0	121484.5
Park94[14]	5.65×10^{-4}	-1	129000
Johnston2014[15]	2.99×10^{-3}	-1	129000
	CO + O $\rightarrow$ C + O_2		
Schwenke2016[65]	1.069×10^{-9}	0.0	82528.6
Park94[14]	6.48×10^{-11}	-0.18	69200
Johnston2014[15]	6.48×10^{-11}	-0.18	69200
	CO + O $\rightarrow$ all products		
Schwenke2016[a]	9.406×10^{-9}	0.0	99238.4

a. Fit over 8500-15,000 K.
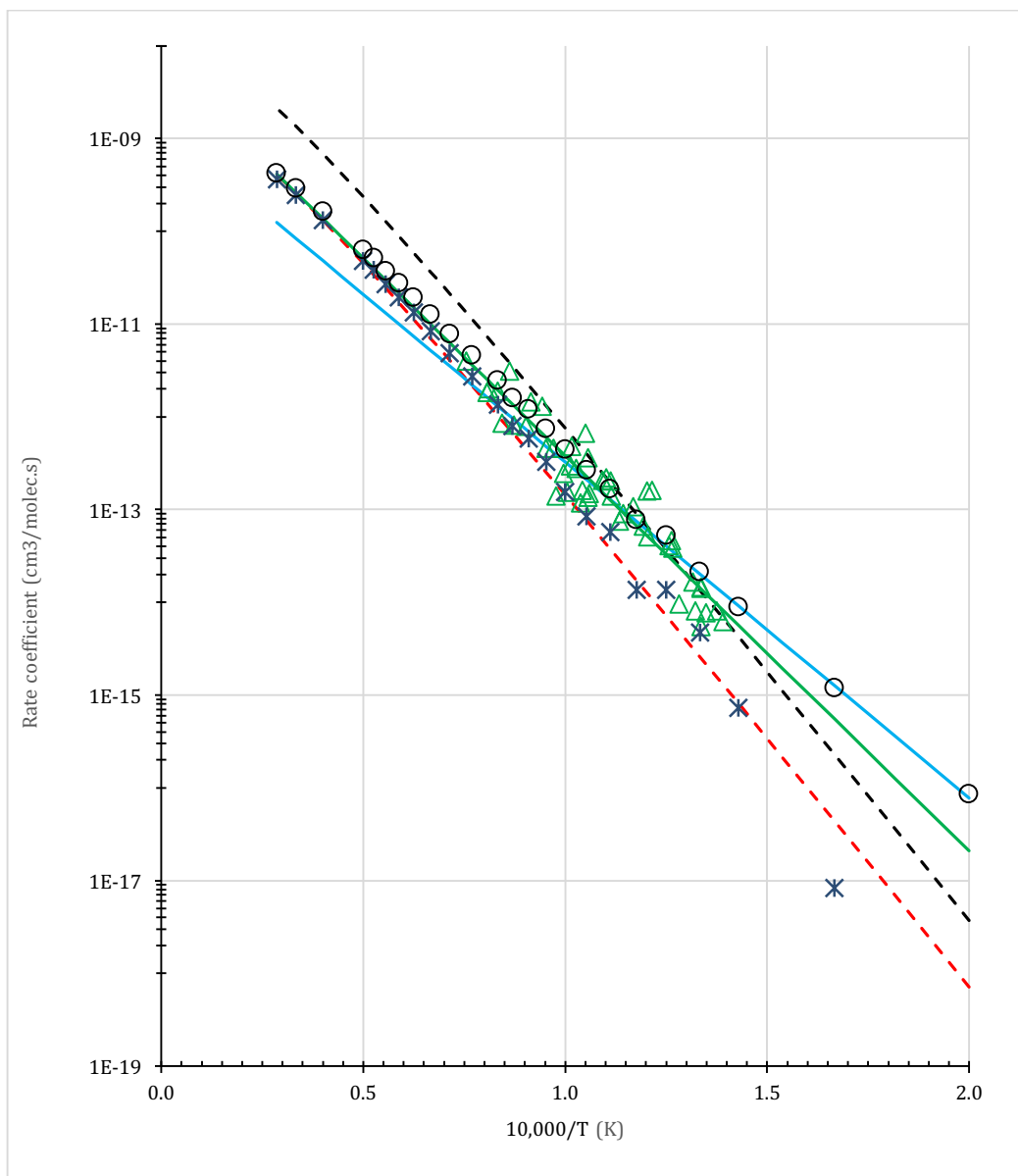
Figure 5. **CO + O thermal dissociation rate coefficients (R5).** Park94 [14] recommendation (red dashed line); Hanson 2-parameter fit [77] (blue line); Appleton data and 2-parameter fit [75] (green triangles and line, respectively); Johnston2014 [15] (black dashed line) and Schwenke2016 [65] QCT dissociation rate coefficients (black stars). QCT combined dissociation and exchange rate coefficients, *i.e.*, total CO removal rate coefficients (open black circles).

IV. Validation of New Parameter Sets by CFD Calculations

Flowfield calculations for the Mars science Laboratory (MSL) entry trajectory, which had an entry speed of 5.85 km/s, have been carried out using the CFD code DPLR [17] to compare the new rate coefficients for CO dissociation and exchange [65] with the Johnston2014 [15] recommendations. The Park94 [14] two-temperature thermochemical nonequilibrium model is used with the following 16 species: CO_2, CO, N_2, O_2, NO, C, N, O, CN, C_2, C^+, O^+, NO^+, O_2^+, CO^+, and e^-. Reference 15 has a complete set of rate coefficients for Mars chemistry, in that it is a set of modifications to the Park94 model and uses the

11

original Park values for the other parameters. For this comparison, the new QCT rate coefficients [65] for CO dissociation and exchange replace the ones in the Park94 model. These calculations are carried out for an atmospheric composition of 96% CO_2 and 4% N_2 at 57 and 72 seconds elapsed time after initial atmospheric entry. The conditions along the surface at the centerline are shown in Figure 6. The pressure, shear, hot wall heat flux and surface temperature are plotted along a line normal to the stagnation line. It can be seen that there is little difference between the model using the QCT rate coefficients [65] (labeled NEW) and the Johnston2014 model (labeled OLD). At this entry speed, the temperature behind the shock is fairly low and there is some residual CO_2 (0.06 mole fraction) and O_2 (0.1 mole fraction) present. O_2 is formed by reaction of CO_2 with O (R2). The 57s result shows no discernable difference between the two chemistry models. Thus, for the MSL trajectory, the details of the nonequilibrium chemistry model do not seem to be important.

Additional calculations have been carried out for the ground tests run at the CUBRC LENS XX reflected shock tunnel for pure CO_2. These tests are described by Hollis *et al*. [78,79] For these tests, the flow impinged on a 12" diameter model in the shape of a typical aeroshell. Figures 7-10 show the comparison of the chemistry models for flow enthalpies of 5.9, 14.3, 20 and 43 MJ/kg, respectively. The surface pressure and cold-wall heat flux are plotted along the model centerline. The Johnston2014 chemistry model [15] and the Park94 model [14] with the Schwenke [65] QCT rate coefficients are compared. At low enthalpy there is no discernable difference between the two models and the CFD results are in good
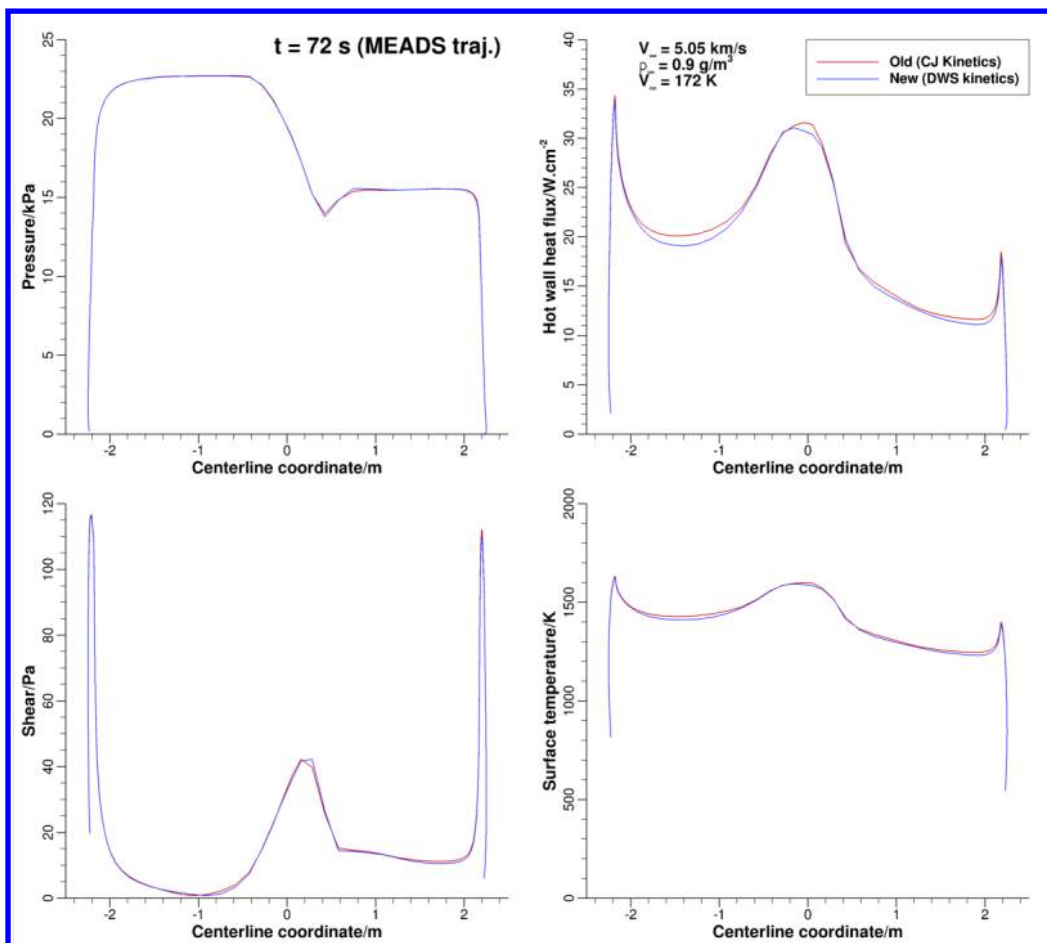

Figure 6. **CFD result near peak heating during the Mars Science Laboratory entry trajectory (72 s from atmospheric entry).** Entry speed was 5.85 km/s. Conditions at the surface shown along centerline. Clockwise from the lower left are shear pressure, pressure, hot wall heat flux and surface temperature. Johnston2014 [15] model in red and Schwenke [65] rate coefficients plus Park94 model [14] in blue.

12

agreement with the measured data. However, at higher enthalpies, the CFD results exhibit larger cold-wall heat fluxes than the measurements and differences between the chemistry models are apparent. Hollis and Prabhu [78,79] posit that the large between CFD and experimental data may be due to several factors, including the modeling of surface catalysis in CFD and errors in the characterization of the free-stream test conditions. These high enthalpy flows are not relevant for Mars entry, which was the focus of the CUBRC test campaign, but would be important for typical Venus entry conditions [5,6].

CFD simulations using the LAURA Navier-Stokes solver [14] have been performed or representative EAST test conditions to compare the Park94 [14] model, the Johnston2014 [15] modification and the QCT rate coefficients [65]. The two-temperature thermochemical nonequilibrium model is applied to a mixture of 96% CO_2 and 4% N_2, treating the same 16 species as used above for MSL. The flowfield simulations are coupled to the radiation simulations through the divergence of the radiative flux, which tends to reduce the peak vibrational-electronic temperature slightly. The HARA nonequilibrium radiation code [20,80] is applied for the radiation computations. The oscillator strengths and electronic level data presented by Babou *et al* [81,82] are applied for the CO 4th Positive, CO IR, and CN Violet band systems. The non-Boltzmann rate model applied in this work was taken from Johnston and Brandis [15].

The shock tube flow is modeled as the flow along the stagnation line of a 5 m radius sphere. This sphere results in a shock standoff distance, omitting the boundary layer, large enough to capture the measurement test lengths. The flow is assumed constant in the direction normal to the shock tube axis,
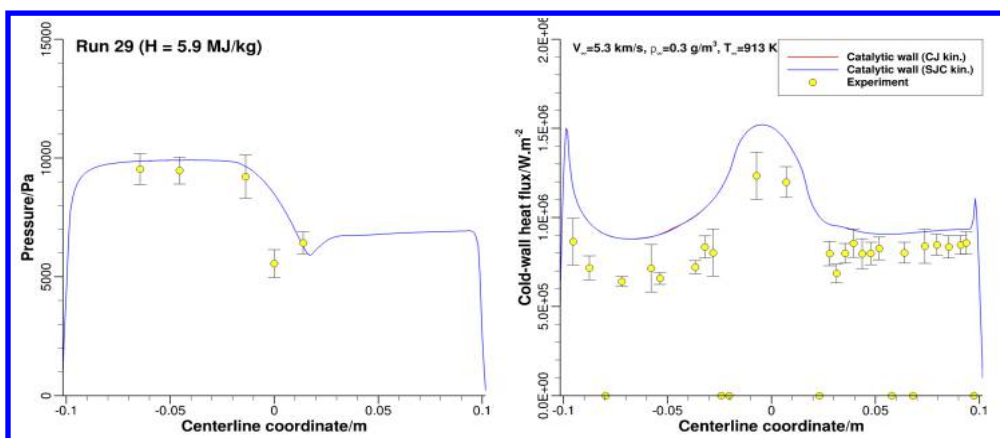

Figure 7. **Comparison of CFD and test data for the LENS XX shock tunnel test at 5.9 MJ/kg enthalpy with pure CO_2.** Shock speed is 5.3 km/s and flow temperature is 913 K. Conditions at the surface shown along centerline. Pressure (left) and cold wall heat flux (right) are shown. Johnston2014 [15] model in red and Schwenke [65] rate coefficients plus Park94 model [14] in blue. LENS data points and error bars are also shown.
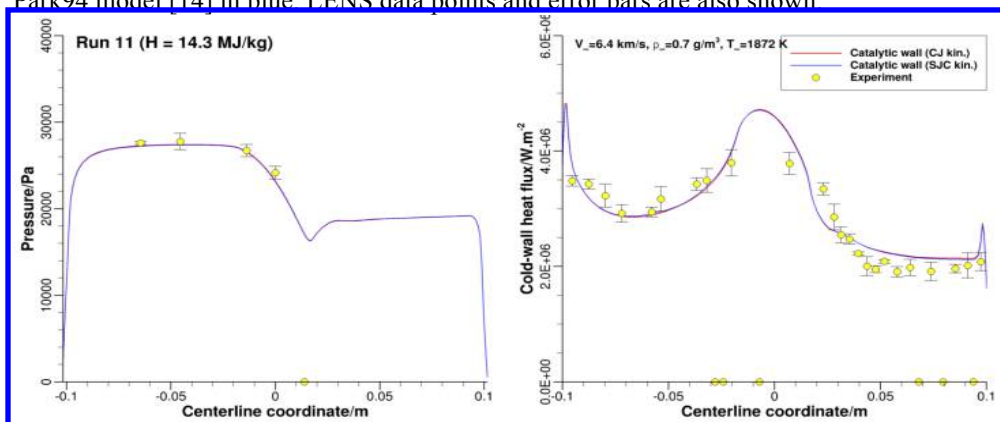

Figure 8. **Comparison of CFD and test data for the LENS XX shock tunnel test at 14.3 MJ/kg enthalpy with pure CO_2.** Shock speed is 6.4 km/s and flow temperature is 1872 K. Additional details same as Figure 7.
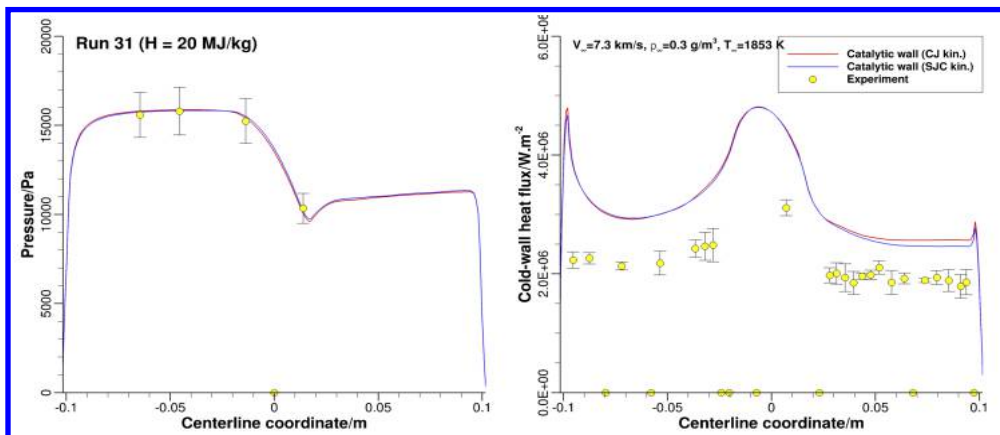
Figure 9. **Comparison of CFD and test data for the LENS XX shock tunnel test at 20 MJ/kg enthalpy with pure CO_2.** Shock speed is 7.3 km/s and flow temperature is 1853 K. Additional details same as Figure 7.
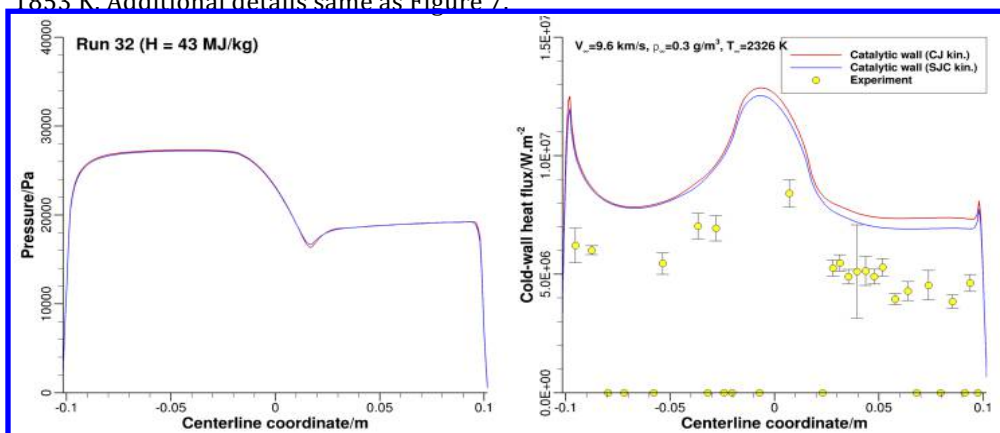

Figure 10. **Comparison of CFD and test data for the LENS XX shock tunnel test at 43 MJ/kg enthalpy with pure CO_2.** Shock speed is 9.6 km/s and flow temperature is 2326 K. Additional details same as Figure 7.

therefore ignoring any boundary layer effects. Brandis *et al*. [83] show that the influence of the boundary layer on the CO 4th Positive and CN Violet bands is negligible for the presently considered wavelength range.

Figures 11-14 compare the measured and simulated radiance for a range of free-stream velocities and densities. For each plot, the horizontal axes are the distance along the stagnation line from the free stream to the surface of the sphere. Spatial convolution functions are applied to the simulations. Two spectral ranges are considered for each case. In each figure, the plot labeled (a) is the integrated intensity from 165- 195 nm which captures the CO 4th Positive band system, while (b) is the comparable quantity for 340-440 nm range, the extent of the CN Violet band system. On each of these plots, the spectral intensity as measured in EAST is given along with the results using the three chemistry models described above. Plots (c) and (d) show the vibrational temperatures and the CO mole fractions from the flow field calculations, respectively. The rate model identified as "This work" applies the CO + M and CO + O rates developed in the present work [61], while retaining the Park *et al*. [10] rates for the remaining rates. The rate models identified as "Park et al. (1994)" and "Johnston and Brandis (2014)" apply to references 14 and 15, respectively. The EAST test conditions are shock speeds of 7.00 and 7.98 km/s at a free stream pressure of 0.1 torr (Fig. 11 and 12, respectively) and 6.43 and 7.82 km/s at a free stream pressure of 0.25 torr (Fig. 13 and 14, respectively). The figures show the data as a function of position an arbitrary reference point in the free stream. The shock front is at 1.0-1.5 cm and the peak intensity, T_v and CO mole fraction is near 2.0 cm.

At the peak in T_v, around 2 cm, the flow is nearly in local thermal equilibrium ($T_v \approx T$) and by 6 cm it is approaching thermal equilibrium.

From the figures, one can see that at the slower shock speeds (7 km/s or less) there is little difference between the temperature and CO mole fraction profiles. At higher shock speeds the temperature is higher than 8000 K and the Johnston2014 model results have lower CO mole fraction than does the modified Park model with the QCT rates for CO + O. In general, the results show that the newer models agree better with the EAST spectral data for CO and CN than does the Park94 model. The rate coefficients in the Johnston model were tuned to optimize that agreement. In contrast, the QCT rate coefficients were not subject to any empirical adjustment. A final assessment of the QCT-based model will be made after completion of rate coefficient calculations for the other important reactions (*i.e.*, CO + CO dissociation and CO + N exchange). It should be noted that the differences between the measured and simulated spectral intensities could be due to other factors besides the reaction rate coefficients, including escape factor modeling and the model used to determine the population of electronically excited species.

V. Summary and Conclusions

This paper represents a summary of results to date of the on-going research effort to develop a physics-based non-equilibrium model for hypersonic entry into the Martian atmosphere as part of the Entry Systems Modeling program in the NASA Space Technology Mission Directorate. The overarching objective is to reduce the model uncertainty in predictions of the convective and radiative heat load experienced by spacecraft during high-speed atmospheric entry. For this approach, we compute potential energy surfaces based on accurate solutions of the electronic Schrödinger equation and reaction cross sections and rate coefficients based on these potentials using quasiclassical trajectory calculations. We have presented new rate coefficients for N_2 dissociation and CO dissociation and exchange. These results illustrate problems and inconsistencies with some of the rate coefficients in the original T-T_v model for Mars entries [14] and with some of the original shock tube data. It is argued that the shock tube experiments of CO + O dissociation did not adequately account for the exchange reaction (R8) that leads to formation of C + O_2. This reaction is the primary channel for CO removal in the shock layer at temperatures below 10,000 K, because the reaction enthalpy for exchange is considerably lower than the comparable value for dissociation. Also, as a result of the present study, the need to compute rate coefficients for CO + CO collisions and the other exchange reactions involving CO + N is apparent. These reactions are currently under study at NASA Ames Research Center.

Comparison of the new rate coefficients with earlier work by Park [14] and Johnston [15] show the effect of the CO removal rate coefficients on reducing the radiative heat flux for Mars entries, and thusly improving agreement between CFD simulations and EAST measurements. However, the effect on convective heating for Mars entries is minimal. It does appear that the effect is significant at higher enthalpic conditions, as would be experienced during Venus entries.
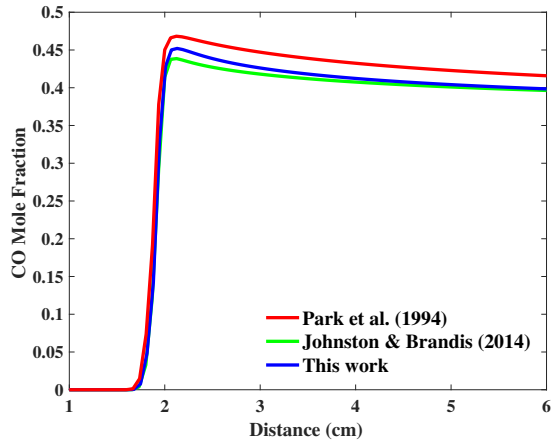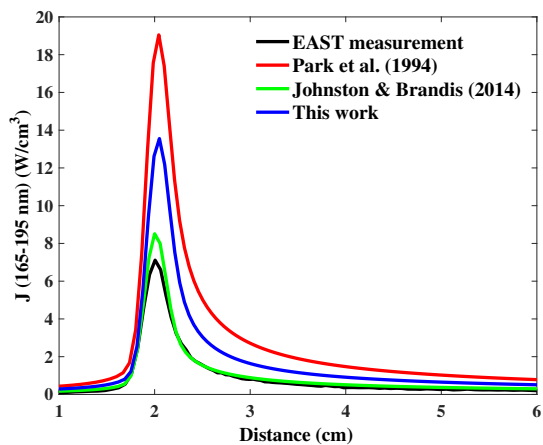
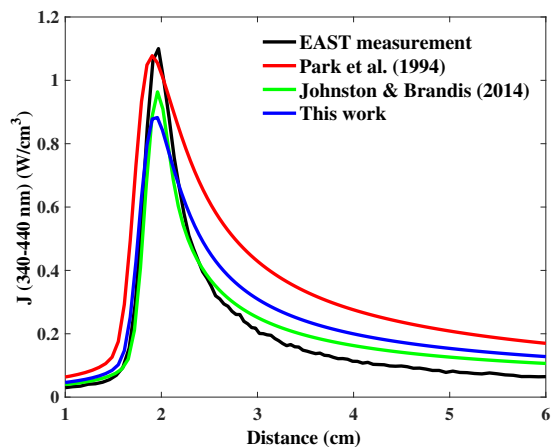**(a) CO 4th Positive**
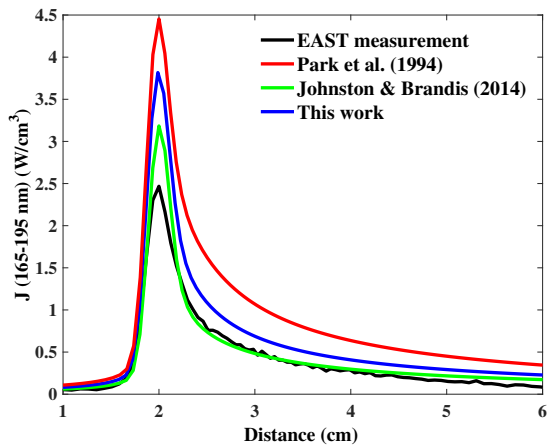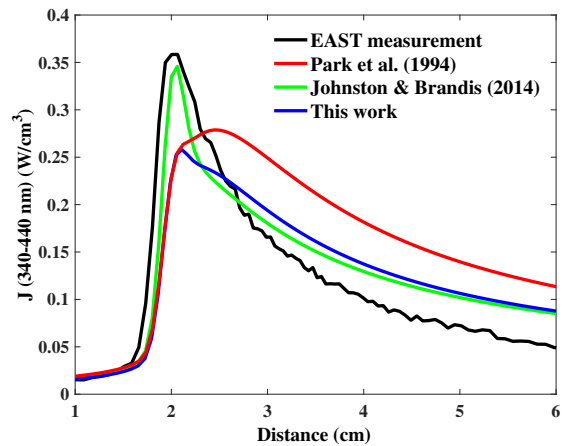
(b) CN Violet
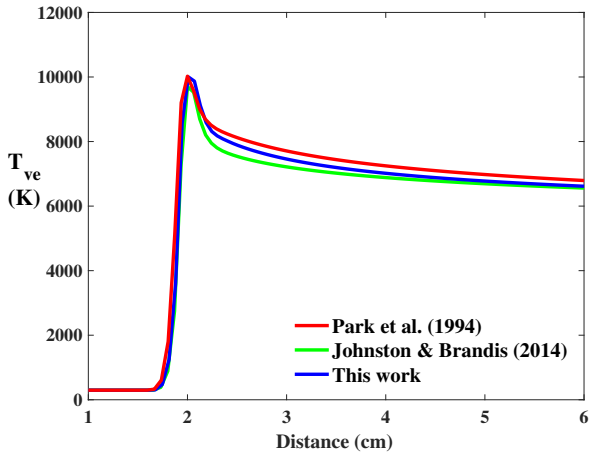
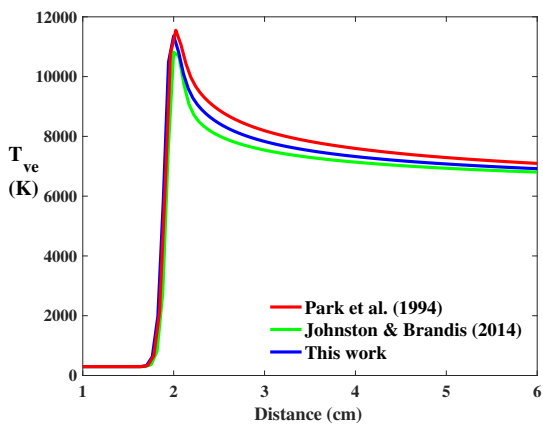**(c) Vibrational-Electronic Temperature**
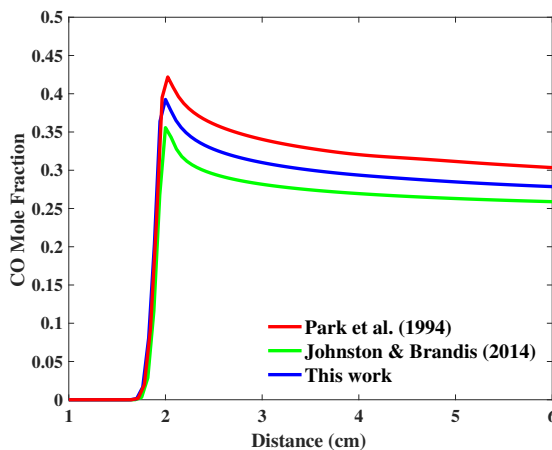
(d) CO Mole Fraction

Figure 11. **Comparison of simulated and measured EAST experiments at 7.00 km/s shock speed and 0.1 Torr free stream pressure.** Data shown for free stream to near equilibration after the shock. Black line are EAST measurements, red line is Park94 model [10] simulation, green line is Johnston2014 [11] simulation and blue line is Park94 model with QCT [61] rate coefficients for CO + O dissociation and exchange reactions.

16

(a) CO 4th Positive

(b) CN Violet

(c) Vibrational-Electronic Temperature

(d) CO Mole Fraction

Figure 12. **Comparison of simulated and measured EAST experiments at 7.98 km/s and 0.1 Torr**. Details are the same as in Figure 11.

(a) CO 4th Positive

(b) CN Violet

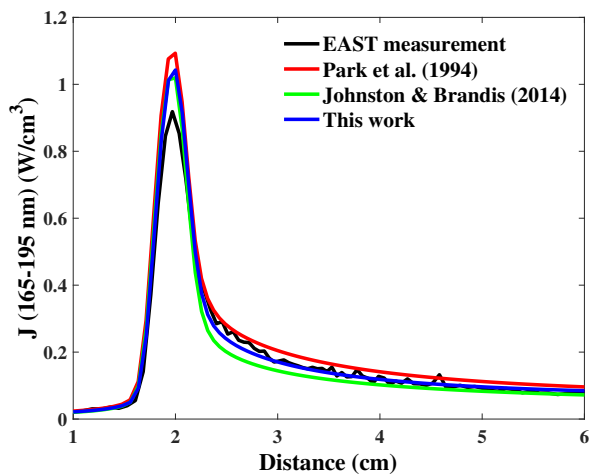**(c) Vibrational-Electronic Temperature**

(d) CO Mole Fraction

Figure 13. **Comparison of simulated and measured EAST experiments at 6.43 km/s and 0.25 Torr.** Details are the same as in Figure 11.

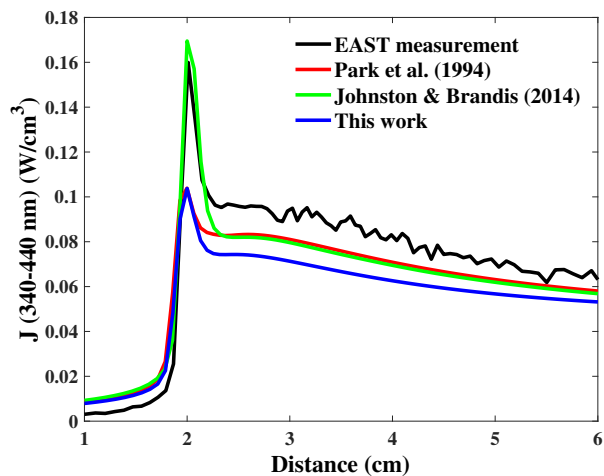18

(a) CO 4ᵗʰ Positive

(b) CN Violet

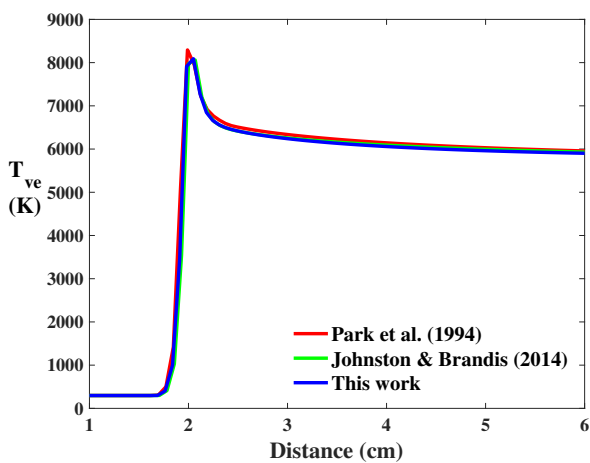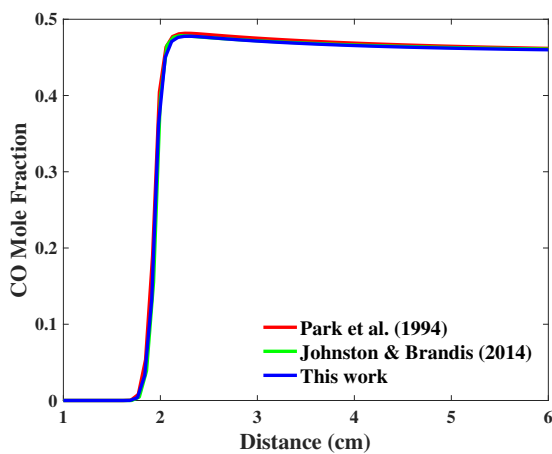**(c) Vibrational-Electronic Temperature**
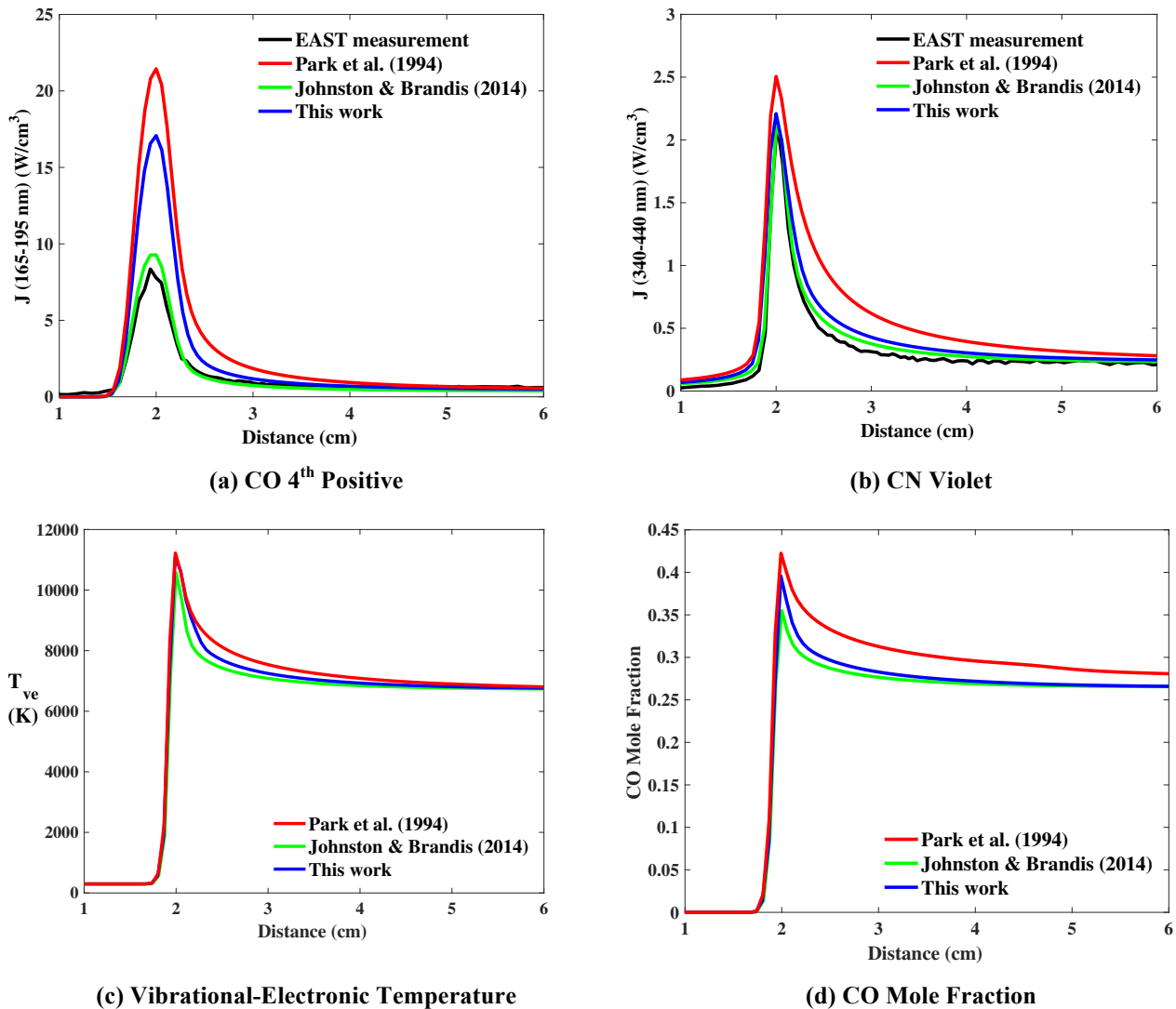
(d) CO Mole Fraction

Figure 14. Comparison of simulated and measured EAST experiments at 7.82 km/s and 0.25 Torr. Details are the same as in Figure 11.

References

1. P. R. Mahaffy, C. R. Webster, S. K. Atreya, H. Franz, M. Wong, P. G. Conrad, D. Harpold, J. J. Jones, L. A. Leshin, H. Manning, T. Owen, R. O. Pepin, S. Squyres, M. Trainer and the MSL Science Team, "Abundance and Isotopic Composition of the Gases in the Martian Atmosphere from the Curiosity Rover", Science **341**, 263-266 (2013).

2. A. Seiff and D. B. Kirk, "Structure of the Atmosphere of Mars at Mid-latitudes", J. Geophys. Res. **82**, 4364-4378 (1977).

3. A. T. Basilevsky and J. W. Heed, "The Surface of Venus," Rep. Prog. Phys. **66** (10), 1699-1734 (2003).

4. H. Suedham, D. U. Titov, F. W. Taylor, and O. Witasse, "Venus a more Earth-like Planet," Nature **450**, 629-632 (2007).

5. K. Fujita, T. Sumi, T. Yamada and N. Ishii, "Assessment of Heating Environment of a Venus Entry Capsule for a Trail Balloon Mission," AIAA 2005-5207 (2005).

19

6. K. Fujita, T. Yamada and N. Ishii, "Impacts of Ablation Gas Kinetics on Hyperbolic Entry Radiative Heating," AIAA 2006-1185 (2006).
7. C. Park, "Radiation Enhancement by Nonequilibrium in Earth's Atmosphere", Spacecraft and Rockets **22** (1), 27-36 (1985).
8. C. Park, "Two-Temperature Interpretation of Dissociation Rate Data for N_2 and O_2", AIAA-88-0458 (1988).
9. C. Park, "Assessment of a Two-Temperature Kinetic Model for Dissociating and Weakly Ionizing Nitrogen", J. Thermophysics **2** (1), 8-16 (1988).
10. C. Park, "Assessment of Two-Temperature Kinetic Model for Weakly Ionizing Air", J. Thermophysics **3** (3), 233-244 (1989).
11. L. Landau and E. Teller, "Theory of Sound Dispersion", Phys. Z. Sowjet. 10, 34 (1936).
12. R. C. Millikan and D. R. White, "Systematics of Vibrational Relaxation", J. Chem. Phys. **39** (12), 3209-3213 (1963).
13. C. Park, "Review of Chemical-Kinetic Problems of Future NASA Missions, I: Earth Entries", J. Thermophysics and Heat Transfer **7** (3), 385-398 (1993).
14. C. Park, J. T. Howe, R. L. Jaffe, and G. V. Candler, "Review of Chemical-Kinetic Problems of Future NASA Missions, II: Mars Entries", J. Thermophysics and Heat Transfer **8** (1), 9-23 (1994).
15. C. O. Johnston and A. M. Brandis, "Modeling of Nonequilibrium CO Fourth-Positive and CN Violet Emission in CO_2-N_2 Gases", J. Quant. Spect. Rad Trans. **149**, 303-317 (2014).
16. B. A. Cruden, D. Prabhu, D. Martinez, H. Lee, D. Bose and J. H. Grinstead, "Absolute radiation measurements in Venus and Mars entry conditions," AIAA-2010-4508 (2010).
17. M. J. Wright, T. White and N. Mangini, "Data Parallel Line Relaxation (DPLR) Code User Manual: Acadia - Version 4.01.1," NASA TM-2009-215388 (2009).
18. A. Mazaheri, P. A. Gnoffo, C. O. Johnston and B. Kleb, "LAURA Users Manual," NASA TM 2010-216836 (2010).
19. E. E. Whiting, Y. Liu, J. O. Arnold, J. A. Paterson, 15. "NEQAIR96, nonequilibrium and equilibrium radiative transport and spectra program: user manual," NASA RP-1389 (1996).
20. C. O. Johnston, B. R. Hollis and K. Sutton, "Spectrum modeling for air shock-layer radiation at lunar return conditions," J. Spacecraft Rockets **45**, 865-78; Non-Boltzmann modeling for air shock-layer radiation at lunar return conditions," J. Spacecraft Rockets **45**, 879-890 (2008).
21. NIST Chemical Kinetics Database Version 7.0, Release 1.6.8 (2015) kinetics.nist.gov/index.jsp
22. L. B. Ibragimova, "Recommended Rate Constants of $CO + O_2 \leftrightarrow CO_2 + O$ Reactions", Khim. Fiz. **10**, 307-310 (1991).
23. K. Thielen and P. Roth, "Stosswelluntersuchungen zum Start der Reaktion $CO + O_2$", Ber. Bunsenges. Phys. Chem. **87**, 920-925 (1983).
24. B. Ruscic, Active Thermochemical Tables (ATcT) values based on ver. 1.118 of the Thermochemical Network (2015); available at ATcT.anl.gov
25. B. Ruscic, R. E. Pinzon, M. L. Morton, G. von Laszewski, S. Bittner, S. G. Nijsure, K. A. Amin, M. Minkoff, and A. F. Wagner, "Introduction to Active Thermochemical Tables: Several 'Key' Enthalpies of Formation Revisited", J. Phys. Chem. A **108**, 9979-9997 (2004).
26. B. Ruscic, R. E. Pinzon, G. von Laszewski, D. Kodeboyina, A. Burcat, D. Leahy, D. Montoya, and A. F. Wagner, "Active Thermochemical Tables: Thermochemistry for the 21st Century", J. Phys. Conf. Ser. **16**, 561-570 (2005).
27. B. Ruscic, "Active Thermochemical Tables: Dissociation Energies of Several Homonuclear First-Row Diatomics and Related Thermochemical Values",
    Theor. Chem. Acc. **133**, 1-12 (2005).
28. S. Gordon and B. J. McBride, Thermodynamic Data to 20000 K for Monoatomic Gases, NASA/TP-1999-208523, (1999).
29. M. W. Chase, Jr., NIST-JANAF Thermochemical Tables, 4th Edition, J. Phys. Chem. Ref. Data, Monograph 9, 1998.
30. L. Gurvich, I. Veyts and C. Alcock, eds., "Thermodynamic Properties of Individual substances", 4th ed. (Hemisphere Publishing Corp., New York, 1989). (English translation of the 1979 Russian edition).
31. R. L. Jaffe, D. W. Schwenke and M. Panesi, "First Principles Calculation of Heavy Particle Rate Coefficients", in "Hypersonic Nonequilibrium Flows: Fundamentals and Recent Advances", E.

Josyula, ed., Progress in Astronautics and Aeronautics, Vol. 247, (AIAA, Reston, VA, 2015), pp 103-158.

32. M. Panesi, R. L. Jaffe, D. W. Schwenke, and T. E. Magin, "Rovibrational internal energy transfer and dissociation of $N_2(^1\Sigma_g^+)$-$N(^4S_u)$ system in hypersonic flows", J. Chem. Phys. **138**, 044312 (2013).

33. A. Munafo, A. Lani, A. Bultel, and M. Panesi, "Modeling of Non-Equilibrium Phenomena in Expanding Flows by means of a Collisional-Radiative Model", Physics of Plasmas 20, 073501, (2013).

34. M. Panesi, A. Munafo, T.E. Magin, and R.L. Jaffe, "Non-equilibrium shock-heated nitrogen flows using a rovibrational state-to-state method" - Physical Review E, Vol.90, No.1, 013009, (2014).

35. A. Munafo, Y. Liu, and M. Panesi "Modeling of dissociation and energy transfer in shock-heated nitrogen flows", Physics of Fluids, 27, 127101, (2015).

36. L. I. Schiff, "Quantum Mechanics", Third Ed. (McGraw-Hill, New York, 1955), 268-279.

37. H. Partridge and D. W. Schwenke, "The determination of an accurate isotope dependent potential energy surface for water from extensive *ab initio* calculations and experimental data," J. Chem. Phys. 106 (11), 4618-4639 (1997).

38. X. Huang , D. W. Schwenke , S. A. Tashkun , and T. J. Lee "An isotopic-independent highly accurate potential energy surface for CO_2 isotopologues and an initial $^{12}C^{16}O_2$ infrared line list," J. Chem. Phys. 136, 124311 (2012).

39. K. Miki, M. Panesi, E. E. Prudencio, S. Prudhomme, "Probabilistic models and uncertainty quantification for the ionization rate of atomic nitrogen," J. Comp. Phys. 231 (9), 3871-3886 (2012).

40. M. Panesi and R. L. Jaffe, unpublished.

41. D. L. Baulch, D. D. Drysdale, J. Duxbury, and S. J. Grant, "Evaluated Kinetic Data for High Temperature Reactions," Volume 3 (Butterworths, London, 1976), 177-202.

42. A. J. C. Varandas and A. A. C. C. Pais, "A realistic double many-body expansion (DMBE) potential energy surface for ground-state O_3 from a multi-property fit to *ab initio* calculations, and to experimental spectroscopic, inelastic scattering, and kinetic isotope thermal rate data," Molec. Phys. **65** (4), 843-860 (1988).

43. M. Bartolomei, E. Carmona-Novillo, M. I. Hernandez, J. Campos-Martinez, and R. Hernandez-Lamoneda, "Global *ab initio* potential energy surfaces for the O_2 $(^3\Sigma_g^-)$ + O_2 $(^3\Sigma_g^-)$ interaction," J. Phys. Chem. **133**, 124311/1-10 (2010).

44. R. Schinke and G. C. McBane, "Photodissociation of ozone in the Hartley band: Potential energy surfaces, nonadiabatic couplings and singlet/triplet branching ratio," J. Chem. Phys. **132**, 044305/16- (2011).

45. R. Dawes, P. Lolur, J. Ma and H. Guo, "Communication: Highly accurate ozone formation potential and implications for kinetics," J. Chem. Phys. **135**, 081102/1-4 (2011).

46. R. Dawes, P. Lolur, A. Li, B. Jiang and H. Guo, "Communication: An accurate global potential energy surface for the ground electronic state of ozone," J. Chem. Phys. **139**, 201103/1-4 (2013).

47. V. G. Tyuterev, R. V. Kochanov, S. A. Tashkun, P. Holka and P. G. Szalay, "New analytical model for the ozone electronic ground state potential surface and accurate *ab initio* vibrational predictions at high energy range," J. Chem. Phys. **139**, 134307/1-22 (2013).

48. D. A. Andrienko and I. D. Boyd, "Rovibrational energy transfer and dissociation in O_2-O collisions," J. Chem. Phys. **144**, 104301/1-19 (2016).

49. I. S. Ulusoy, D. A. Andrienko, I. D. Boyd and R. Hernandez, "Quantum and quasiclassical collisional dynamics of O_2-Ar at high temperatures," J. Chem. Phys. **144**, 234311/1-11 (2016).

50. D. A. Andrienko and I. D. Boyd, "Thermal relaxation of molecular oxygen in collisions with nitrogen atoms", J. Chem. Phys., **145**, 014309/1-14 (2016).

51. Z. Varga, R. Meana-Paneda, G. Song Y. Paukku and D. G. Truhalr, "Potential energy surface of triplet N_2O_2," J. Chem. Phys. 144, 024310/1-14 (2016).

52. R. Jaffe, D. Schwenke and G. Chaban, Vibrational and Rotational Excitation and Dissociation in N_2-N_2 Collisions from Accurate Theoretical Calculations," AIAA 2010-4517 (2010).

53. R. L. Jaffe, D. W. Schwenke, M. Grover, P. Valentini, T. E. Schwartzentruber, S. Venturi and M. Panesi, Comparison of quantum mechanical and empirical potential energy surfaces and computed rate coefficients for N_2 dissociation," AIAA 2016-0503 (2016).

54. Y. Paukku, K. R. Yang, Z. Varga and D. G. Truhlar, "Global *ab initio* ground-state potential energy surface of N_4," J. Chem. Phys. **139**, 044309/1-8 (2013).

55. J. D. Bender, P. Valentini, I. Nompelis, Y. Paukku, Z. Varga, D. G. Truhlar, T. Schwartzentruber, and G. V. Candler, "An Improved Initio Potential Energy Surface and Multi-Temperature Trajectory Calculations of $N_2 + N_2$ Dissociation Reactions," J. Chem. Phys. **143**, 054304 (2015).

56. P. Gamallo, M. Gonzalez and R. Sayos, "*Ab initio* study of the two lowest triplet potential energy surfaces involved in the N (^{4}S) + NO ($X\,^2\Pi$) reaction," J. Chem. Phys. **118** (23), 10602-10610 (2003).

57. P. Gamallo, M. Gonzalez and R. Sayos, "*Ab initio* derived analytical fits of the two lowest triplet potential energy surfaces and theoretical rate coefficients for the N (^{4}S) + NO ($X\,^2\Pi$) system," J. Chem. Phys. **119** (5), 2545-2556 (2003).

58. P. Gamallo, R. Martinez, R. Sayos and M. Gonzalez, Quasiclassical dynamics and kinetics of the N + NO → N_2 + O, NO + N atmospheric reactions," J. Chem. Phys. **132**, 1344303/1-9 (2010).

59. S. Akpinar, I. Armenise, P. Defazio, F. Esposito, P. Gamallo, C. Petrongolo and R. Sayos, "Quantum mechanical and quasiclassical Born-Oppenheimer dynamics of the reaction N_2 ($^1\Sigma_g^+$) + O (^{3}P) → N(^{4}S) + NO ($X\,^2\Pi$) on the N_2O $a\,^3$A" and $b\,^3$A' surfaces," Chem. Phys. **398**, 81-89 (2012).

60. W. Lin, Z. Varga, G. Song, Y. Paukku and D. G. Truhlar, "Global triplet potential energy surfaces for the N_2 ($X\,^1\Sigma_g^+$) + O (^{3}P) → NO ($X\,^2\Pi$) + N (^{4}S) reaction," J. Chem. Phys. **144**, 024309/1-11 (2016).

61. W. Lin, R. Meana-Paneda, Z. Varga, and D. G. Truhlar, "A quasiclassical trajectory study of the N_2 ($X\,^1\Sigma_g^+$) + O (^{3}P) → NO ($X\,^2\Pi$) + N (^{4}S) reaction," J. Chem. Phys. **144**, 024314 (2016).

62. R. Sayos, C. Oliva and M. Gonzalez, "New analytical (^{2}A', ^{4}A') surfaces and theoretical rate coefficients for the N (^{4}S) + O_2 reaction," J. Chem. Phys. **117** (2) 670-679 (2002).

63. J. He, F. Cheng and J. Lim, "A quasiclassical trajectory study for the N (^{4}S) + O_2 ($X\,^3\Sigma_g^-$) → NO ($X\,^2\Pi$) + O (^{3}P) reaction on the new ^{2}A' and ^{4}A' potential energy surfaces," J. Chem. Phys. **124**, 054303/1-9 (2006).

64. J. C. Carlos-Palacio, R. J. Bemish and M. Meuwly, "Communication: Equilibrium rate coefficients from atomistic simulations: the O (^{3}P) + NO ($^2\Pi$) → O_2 ($X\,^3\Sigma_g^-$) + N (^{4}S) reaction at temperatures relevant to the hypersonic flight regime," J. Chem. Phys. **142**, 091104/1-4 (2015).

65. D. W. Schwenke, R. L. Jaffe and G. M. Chaban, "Collisional dissociation of CO: *ab initio* potential energy surfaces and quasiclassical trajectory rate coefficients," J. Chem. Phys., submitted (2016).

66. O. Yazidi, H. Gritli and G. Chambaud, "Electronic structure and reactivity of the CNO/NCO/CON isomers," Mol. Phys. **103**, 3321-3336 (2005).

67. S. Andersson, N. Markovic and G. Nyman, "An inproved potential energy surface for the C + NO reaction," Phys. Chem. Chem. Phys. **2**, 613-620 (2000).

68. S. Andersson, N. Markovic and G. Nyman, Quasi-classical trajectory simulations of C + NO crossed molecular beam experiments," Chem. Phys. **259**, 99-108 (2000).

69. E. Abrahamsson, S. Andersson, N. Markovic and G. Nyman, "A new reaction path for the C + NO reaction: dynamics on the ^{4}A" potential-energy surface," Phys. Chem. Chem. Phys. **10**, 4400-4409 (2008).

70. J. P. Appleton, M. Steinberg and D. J. Liquornick, "Shock-tube study of nitrogen dissociation using vacuum-ultraviolet light absorption," J. Chem. Phys. **48**, 599-608 (1968).

71. R. Hanson and D. Baganoff, Shock-tube study of nitrogen dissociation rates using pressure measurements," AIAA J. **10** (2), 211-215 (1972).

72. D. Kewley and H. Hornung, "Free-piston shock-tube study of nitrogen dissociation," Chem. Phys. Lett. **25**, 531-536 (1974).

73. K. Thielen and P. Roth, "N atom measurements in high-temperature N_2 dissociation kinetics," AIAA J. **24** (7), 1102-1105 (1986).

74. W. O. Davies, "Radiative energy transfer on entry into Mars and Venus,", IITRI-T200-8, Illinois Institute of Technology, Chicago, IL, NASA CR-58574 (1964).

75. J. P. Appleton, M. Steinberg and D. J. Liquornick, "Shock-tube study of carbon monoxide dissociation using vacuum-ultraviolet light absorption," J. Chem. Phys. **52**, 2205-2221 (1970).

76. H.-J. Mick, M. Burmeister and P. Roth, "Atomic resonance absorption spectroscopy measurements on high-temperature CO dissociation kinetics," AIAA J. **31** (4), 671-676 (1993).

77. R. K. Hanson, "Shocktube study of carbon monoxide dissociation kinetics," J. Chem. Phys. **60**, 4970-4976 (1974).

22

78. B. R. Hollis and D. K. Prabhu, "Assessment of laminar, convective aeroheating prediction uncertainties for Mars entry vehicles," AIAA2011-3144 (2011).
79. B. R. Hollis, D. K. Prabhu, M. Maclean and A. Dufrene, "Blunt-body aerothermodynamic database from high-enthalpy CO_2 testing in an expansion tunnel," AIAA 2016-4141 (2016).
80. C. O. Johnston, B. Hollis, K. Sutton, "Non-Boltzmann Modeling for Air Shock Layers at Lunar Return Conditions", Journal of Spacecraft & Rockets, **45**, 879–890 (2008).
81. Y. Babou, P. Riviere, M.-Y. Perrin, A. Soufiani, "High Temperature and Nonequilibrium Partition Function and Thermodynamic Data of Diatomic Molecules", International Journal of Thermophysics, **30**, 416–438 (2009).
82. Y. Babou, P. Riviere, M.-Y. Perrin, A. Soufiani, "Spectroscopic Data for the Prediction of Radiative Transfer in CO_2-N_2 Plasmas", J. Quant. Spect. Rad Trans. **110**, 89-108 (2009).
83. A. M. Brandis, C. O. Johnston, B. A. Cruden, D. K. Prabhu, A. A. Wray, Y. Liu, D. W. Schwenke, D. Bose, "Validation of CO 4th Positive Radiation for Mars Entry", Journal of Quantitative Spectroscopy and Radiative Transfer, **121**, 91–104 (2013).